

The Allosteric Role of the Ca^{2+} Switch in Adhesion and Elasticity of C-Cadherin

Marcos Sotomayor and Klaus Schulten

Department of Physics, University of Illinois at Urbana-Champaign, and Beckman Institute for Advanced Science and Technology, Urbana, Illinois

ABSTRACT Modular proteins such as titin, fibronectin, and cadherin are ubiquitous components of living cells. Often involved in signaling and mechanical processes, their architecture is characterized by domains containing a variable number of heterogeneous “repeats” arranged in series, with either flexible or rigid linker regions that determine their elasticity. Cadherin repeats arranged in series are unique in that linker regions also feature calcium-binding motifs. While it is well known that the extracellular repeats of cadherin proteins mediate cell-cell adhesion in a calcium-dependent manner, the molecular mechanisms behind the influence of calcium in adhesion dynamics and cadherin’s mechanical response are not well understood. Here we show, using molecular dynamics simulations, how calcium ions control the structural integrity of cadherin’s linker regions, thereby affecting cadherin’s equilibrium dynamics, the availability of key residues involved in cell-cell adhesion, and cadherin’s mechanical response. The all-atom, multi-nanosecond molecular dynamics simulations involved the entire C-cadherin extracellular domain solvated in water (a 345,000 atom system). Equilibrium simulations show that the extracellular domain maintains its crystal conformation (elongated and slightly curved) when calcium ions are present. In the absence of calcium ions, however, it assumes a disordered conformation. The conserved residue Trp², which is thought to insert itself into a hydrophobic pocket of another cadherin molecule (thereby providing the basis for cell-cell adhesion), switches conformation from exposed to intermittently buried upon removal of calcium ions. Furthermore, the overall mechanical response of C-cadherin’s extracellular domain is characterized at low force by changes in shape (tertiary structure elasticity), and at high force by unraveling of secondary structure elements (secondary structure elasticity). This mechanical response is modulated by calcium ions at both low and high force, switching from a stiff, rod-like to a soft, spring-like behavior upon removal of ions. The simulations provide an unprecedented molecular view of calcium-mediated allostery in cadherins, also illustrating the general principles of linker-mediated elasticity of modular proteins relevant not only for cell-cell adhesion and sound transduction, but also muscle elasticity.

INTRODUCTION

Development of complex multicellular organs and tissues relies on selective and robust adhesion between cells (1–4). Cadherin proteins are responsible for calcium-mediated cell-cell adhesion and have been implicated in various biologically relevant processes related to tissue morphogenesis and maintenance of tissue integrity, such as neuronal connectivity or prevention of tumor cell propagation (3–8). Members of the cadherin family of proteins have also been suggested to form part of the mechanotransduction apparatus of the inner ear (9–12). Classical cadherins feature a cytoplasmic domain, a single transmembrane segment, and a long extracellular domain made of five, tandemly arranged, heterogeneous cadherin repeats (1,13–15). The repeats are labeled EC1–EC5, with EC1 being the most distant from the membrane (see Fig. 1 A).

Selective adhesion is achieved through *trans* interactions between cadherin extracellular domains coming from two adjacent cells (8,15,16). In addition, *cis* interactions arising from dimerization of cadherin molecules that belong to the same cell have been suggested to be necessary for the for-

mation of *trans* bonds (16–22). The interaction between cadherin extracellular domains likely involves one or more repeats from each cadherin molecule (8,23–29). Multiple studies using different experimental techniques such as mutagenesis, electron microscopy, force measurements, NMR, and x-ray crystallography have been used to postulate and probe different models of *trans*- and *cis*- interactions (see (8) for a recent review). In all cases it has been shown that Ca^{2+} and the EC1 repeat are both essential for at least the initial stages of *trans*-bond formation.

Calcium ions seem to stabilize and rigidify extracellular domains. Indeed, electron microscopy (EM) and other experiments have shown that the E-cadherin extracellular domain forms an elongated, semicurved rod in the presence of Ca^{2+} , while it collapses upon Ca^{2+} removal (17,30–34). The crystal structure of a complete C-cadherin extracellular domain (35) depicts in atomic detail the elongated rod observed for E-cadherin with EM and also reveals all Ca^{2+} binding spots found in linker regions between repeats (Fig. 1 A). Biochemical assays, mutagenesis, and quantitative force and bead aggregation measurements have shown that disruption of some Ca^{2+} binding spots cooperatively influence large regions of the protein structure, often abolish adhesion, and affect the stability of individual repeats (36–38). Furthermore, molecular dynamics simulations of a single C-cadherin

Submitted November 10, 2007, and accepted for publication January 22, 2008.

Address reprint requests to Klaus Schulten, E-mail: kschulte@ks.uiuc.edu.

Editor: Angel E. Garcia.

© 2008 by the Biophysical Society
0006-3495/08/06/4621/13 \$2.00

doi: 10.1529/biophysj.107.125591

repeat's mechanical unfolding and of the EC1-EC2 E-cadherin equilibrium dynamics have confirmed the relevant role of Ca^{2+} in the stability of cadherin repeats (39–41).

While calcium ions provide rigidity, the EC1 repeat provides an anchor residue (Trp^2) that may intramolecularly dock into a hydrophobic pocket of EC1, or insert itself into the same hydrophobic pocket but of a neighboring EC1 coming from an adjacent cell, thereby facilitating cell-cell adhesion (17,33,35,42–44). Antibody binding and mutagenesis combined with force measurements suggest that Ca^{2+} binding allosterically modulates the availability of Trp^2 (38,45). However, a molecular dynamic view of how calcium ions control Trp^2 availability and the flexibility of cadherin repeats is missing. Here we present molecular dynamics simulations that reveal how Ca^{2+} controls the elasticity and adhesive property of C-cadherin, switching the cadherin ectodomain's mechanical response from a stiff, rod-like regime to one that is soft and spring-like. Moreover, the simulations depict, for the first time at the atomic level, the Ca^{2+} modulation of Trp^2 availability.

METHODS

Systems

The *psfgen* VMD (46) plug-in was utilized to build four systems containing the entire crystal structure of C-cadherin (Protein Data Bank code 1L3W) solvated in water with the VMD *solvate* plug-in. The first system with a total of 345,467 atoms included 12 crystallographically resolved and protein-bound Ca^{2+} ions and eight bulk Na^+ ions randomly placed for cell neutralization with the *autoionize* VMD plug-in. The second system encompassing 345,407 atoms did not include Ca^{2+} ions, but contained 32 bulk Na^+ ions. The last two systems included 12 K^+ or Na^+ ions replacing crystallographically resolved Ca^{2+} ions, respectively. In addition, these two systems included 20 bulk Na^+ ions and encompassed 345,443 atoms. In all systems, 39 crystallographic water molecules were kept as part of the model while *n*-acetylglucosamine residues were excluded. Disulfide bonds for cysteines 448–532 and 530–539 were explicitly modeled for all systems. Residues Asp, Glu, Lys, and Arg were assumed to be charged throughout the protein, while the protonation states of His residues were chosen favoring the formation of evident hydrogen bonds. Before solvation, the C-cadherin molecule was spatially aligned such that the vector joining the C_α atoms of the terminal residues was oriented along the *x* axis. The size of the resulting systems was $\sim 36.4 \times 10.5 \times 9.4 \text{ nm}^3$.

Molecular dynamics simulations

All molecular dynamics simulations were performed using NAMD 2.6 (47), the CHARMM22 force field for proteins with the CMAP correction (48–50) (see validation using lysozyme (51,52) in Supplementary Materials, Data S1, Fig. S23), and the TIP3P model for water (53). The standard set of CHARMM parameters for ions was utilized in all simulations. Parameters for Ca^{2+} correspond to those obtained to reproduce their experimental free energy of hydration (54). Parameters for K^+ and Na^+ did not include the NBFIX correction, used in simulation of potassium ion channels to describe ion-backbone interactions more accurately, as C-cadherin Ca^{2+} binding sites involve ion-backbone as well as ion-to-side-chain interactions. A summary of all simulations carried out in our study totaling >150 ns is presented in Table 1.

A uniform integration time step of 1 fs was assumed for all types of interactions throughout all simulations. In all cases a cutoff of 12 Å (switching

function starting at 10 Å) for van der Waals interactions was assumed, and the particle-mesh Ewald method was used to compute long-range electrostatic forces without cutoff (55). The density of grid points for particle-mesh Ewald was at least $1/\text{Å}^3$. Periodic boundary conditions were assumed in all cases.

Langevin dynamics was utilized to maintain a constant temperature of $T = 300 \text{ K}$ when indicated, with the damping coefficient set to 5 or 0.1 ps^{-1} for all heavy atoms (see Table 1). Constant-pressure simulations at 1 atm were conducted using a hybrid Nosé-Hoover-Langevin piston method with a decay period of 200 fs and a damping timescale of 50 fs.

Constant velocity stretching simulations were performed using the steered molecular dynamics method (SMD) and the NAMD Tcl Forces interface. The stretching direction was set along the *x* axis, which matched the vector connecting the C_α atoms of the N- and C-terminal residues when the systems were built. The SMD simulations were performed by attaching the C_α^1 and C_α^{540} atoms of the N- and C-terminal residues to virtual (independent) springs of stiffness $k_s = 1 \text{ (kcal/mol)/\AA}^2$ each. The free ends of the mentioned virtual springs were then moved away from the protein at a constant velocity of *v* each in opposite directions. Different velocities were used throughout simulations (see Table 1). The force applied at each end was computed using the extension of the virtual springs.

Two additional SMD protocols were used. In the first protocol, the center of mass of all C_α atoms of repeats EC1 and EC3 (SimCa10) or repeats EC3 and EC5 (SimCa11) were each attached to virtual springs of stiffness $k_s = 1 \text{ (kcal/mol)/\AA}^2$ each. The free ends of the springs were moved as in the standard SMD protocol described above, effectively stretching repeats EC2 and EC4 (see Data S1, Fig. S19).

The second SMD protocol (length clamp) consisted of two phases. First, a standard constant velocity SMD simulation is performed in which one end of the protein (C_α atom of C- or N-terminus) is held fixed while the other end of the protein (C_α atom of N- or C-terminus) is pulled by a virtual spring as described above. The second phase begins when a predetermined elongation has been achieved. Then, the free end of the virtual spring is held fixed in space and the protein is allowed to relax while the force applied on the spring by the protein is obtained by monitoring the extension of the virtual spring.

Analysis tools

Coordinates of all atoms of the system were saved every picosecond of simulation for later analysis. Overall structural deformation of the protein was monitored by computing root mean-square deviations (RMSD) over entire trajectories using VMD. The crystallographic structure served as the reference point, and positions of protein C_α atoms were compared. End-to-end distances were computed as the distance between the C_α atoms of the N- and C-terminal residues. Root mean-square fluctuations (RMSF) of C_α atom positions were computed using VMD and trajectories in which each cadherin repeat (EC1–EC5) was individually aligned to its crystal conformation. Alignment of structures for visualization purposes and for computation of RMSD or RMSF was performed by comparing positions of C_α atoms to their original positions in the crystal using the VMD Tcl interface. The solvent-accessible surface area for Trp^2 was computed using VMD and assuming a probe radius of 0.14 nm.

The total energy E_T of the system (reported as TOTAL3 in the NAMD output) was computed using the total potential energy U , the total kinetic energy K_c obtained from step-centered velocities ($v_{ci}^2 = [(x_{i+1} - x_{i-1})/2\Delta t]^2$), and the total kinetic energy K_h obtained from half-step velocities averaged ($v_{hi}^2 = [(x_i - x_{i-1})/\Delta t]^2 + [(x_{i+1} - x_i)/\Delta t]^2$)/2). The final form of E_T used was

$$E_T = U + \frac{2}{3}K_c + \frac{1}{3}K_h - \frac{4}{3}(K_h - K_c) + \frac{4}{3}\langle K_h - K_c \rangle, \quad (1)$$

where the first three terms correspond to a total energy that is numerically well behaved in long timescales, while the last two terms correct short-timescale fluctuations with a weighted exponential average ($\langle X \rangle_{\text{new}} = 0.9375 \langle X \rangle_{\text{old}} + 0.0625 X$).

TABLE 1 Summary of simulations

Label	t_{sim} (ns)	Type	Ensemble	γ (ps ⁻¹)	Velocity (nm/ns)	Start
SimCa1	10.00	EQ	NpT/NVE*	—	—	—
SimCa2	0.67	PCV	NV	—	5 × 2	SimCa1 (5.0 ns)
SimCa2E	1.07	PCV	NV	—	5 × 2	SimCa2
SimCa3	10.00	REL	NVE	—	—	SimCa2
SimCa4	4.04	EQ	NpT	5.0	—	SimCa1 (1.1 ns)
SimCa5	1.70	PCV	NpT	5.0	5 × 2	SimCa4
SimCa6	2.15	PCV	NpT	0.1	5 × 2	SimCa4
SimCa7	0.50	PCV	NV	—	50 × 2	SimCa1 (5.0 ns)
SimCa8	0.50	PCV	NV	—	25 × 2	SimCa1 (5.0 ns)
SimCa9	14.96	PCV	NV	—	0.5 × 2	SimCa1 (5.0 ns)
SimCa10	1.30	PCV [†]	NV	—	5 × 2	SimCa1 (5.0 ns)
SimCa11	1.30	PCV [†]	NV	—	5 × 2	SimCa1 (5.0 ns)
SimCa12	5.00	PCL	NV	—	10/13 nm/C	SimCa1 (5.0 ns)
SimCa13	5.00	PCL	NV	—	10/8 nm/C	SimCa1 (5.0 ns)
SimCa14	3.60	PCL	NV	—	10/15 nm/C	SimCa1 (5.0 ns)
SimCa15	2.90	PCL	NV	—	10/13 nm/N	SimCa1 (5.0 ns)
SimCa16	2.30	PCL	NV	—	10/14 nm/N	SimCa1 (5.0 ns)
SimCa17	3.10	PCL	NV	—	10/8 nm/N	SimCa1 (5.0 ns)
SimApo1	10.00	EQ	NpT/NVE*	—	—	—
SimApo2	0.65	PCV	NV	—	5 × 2	SimApo1 (5.0 ns)
SimApo2E	1.05	PCV	NV	—	5 × 2	SimApo2
SimApo3	5.00	REL	NVE	—	—	SimApo2
SimApo4	9.34	EQ	NpT	5.0	—	SimApo1 (1.1 ns)
SimApo5	14.61	EQ	NpT	0.1	—	SimApo1 (1.1 ns)
SimApo6	2.00	PCV	NpT	5.0	5 × 2	SimApo1 (5.0 ns)
SimApo7	2.10	PCV	NpT	0.1	5 × 2	SimApo1 (5.0 ns)
SimApo8	12.10	PCV	NV	—	0.5 × 2	SimApo1 (5.0 ns)
SimApo9	3.40	PCL	NV	—	10/8 nm/C	SimApo1 (5.0 ns)
SimK1	10.00	EQ	NpT/NVE*	—	—	—
SimK2	5.00	EQ	NpT/NVE*	—	—	—
SimNa1	10.00	EQ	NpT/NVE*	—	—	—
SimNa2	1.77	PCV	NV	—	5 × 2	SimNa1 (5.0 ns)

Labels indicate the presence (Ca) or absence (Apo) of crystallographic Ca²⁺ ions in the system. Replacement of Ca²⁺ by Na⁺ or K⁺ is indicated by labels Na and K, respectively. EQ denotes equilibrium simulations, PCV denotes constant velocity SMD simulations, and REL denotes free dynamics simulations in the corresponding ensemble. PCL denotes constant velocity SMD simulations in which one end of the protein is held fixed while the other end of the protein (N- or C-terminus) is pulled until a predefined elongation has been achieved. Then, the steering atom is held in space and the protein is allowed to relax in a so-called length-clamp steering protocol (see Methods). Initial coordinates and velocities were obtained from the last frame of the simulations mentioned in the *Start* column. All SMD simulations were performed by attaching steering springs to C_α atoms of residues 1 and 540, unless otherwise stated.

*These simulations consisted of 1000 steps of minimization, 100 ps of dynamics with the backbone of the protein restrained ($k = 1$ Kcal/mol/Å²), and the remaining time as free dynamics in the NpT (1 ns with $\gamma = 5$ ps⁻¹) and NVE ensembles.

[†]These SMD simulations were performed by pulling repeats one and three (SimCa10) or three and five (SimCa11) in opposite directions (see Methods).

Local deformations or strain (see Supplementary Material, [Movie S1](#), movies mIII and mIV) were computed following a method similar to that described in Ortiz et al. (56). First, for each C_αⁱ atom of the protein, a list of neighboring C_α^j atoms (within 1 nm) was created using positions of the crystal conformation. Then, the local strain $u_i(t)$ was computed every time frame (t) for every C_αⁱ atom using

$$u_i(t) = \frac{1}{N_i} \sum_j \frac{|\vec{r}_j(t) - \vec{r}_i(t)|}{|\vec{r}_j(0) - \vec{r}_i(0)|}, \quad (2)$$

where $\vec{r}_i(t)$ is the position of the C_α atom i at time t and N_i is the total number of neighboring C_α^j atoms for C_α atom i (determined as described above). The strain value $u_i(t)$ was then used to color each C_α atom.

RESULTS

Molecular dynamics simulations were carried out using the complete extracellular domain of C-cadherin, a *Xenopus* cadherin involved in the processes that drive morphogenesis

during amphibian gastrulation (57). The corresponding crystal structure (35), solved at 3.1 Å resolution (PDB code 1L3W), features five cadherin repeats, each made of ~110 amino acids and folded in a Greek-key motif characterized by seven β-strands forming two β-sheets (13). Four sets of simulations of this structure were performed. The first set (labeled “SimCaX”) utilized a system containing the protein, water molecules, and 12 crystallographically resolved Ca²⁺ ions (three ions located at each linker region). The second set (labeled “SimApoX”) was performed without Ca²⁺ ions. The last two sets, labeled “SimKX” and “SimNaX”, involved systems in which crystallographically resolved Ca²⁺ ions were replaced by potassium (K⁺) and sodium (Na⁺) ions, respectively (Fig. 2). Further details of the systems and simulations can be found in Methods and [Data S1](#).

Influence of ions on C-cadherin equilibrium dynamics

Equilibrium simulations showed that the overall curved shape of the protein was maintained throughout 10 ns of dynamics in which Ca^{2+} ions were present in the model (SimCa1, Fig. 1 *C*), while the cadherin extracellular domain adopted a disordered shape when calcium ions were removed (SimApo1, Fig. 1 *D*). Indeed, the absence of Ca^{2+} resulted in strong repulsion between negatively charged residues (previously coordinating ions) and partial disruption of linker regions (Fig. 2 *B*). Complete disruption and unfolding of linker regions was prevented by performing an equilibration step in which 1000 steps of minimization and 100 ps of dynamics were carried out with backbone atoms harmonically restrained to their crystal conformation (as in all our initial equilibrations, see Methods and Table 1). The linker disruption, most clearly seen at the linker between EC3 and EC4, favored independent motion of individual repeats leading to the observed disordered shape (Fig. 3). The same behavior was reproduced in simulations that used different temperature control protocols (SimCa4, SimApo4, and SimApo5; Data S1, Figs. S8 and S9). Whether protonation states of charged amino acids change upon Ca^{2+} removal remains to be elucidated. However, our results are in agreement with experiments showing that linkers without calcium can destabilize cadherin repeats through electrostatic interactions (37). Additional simulations were performed in which Ca^{2+} ions were replaced by K^+ or Na^+ ions (SimK1 and SimNa1, respectively). The replacement of divalent ions by monovalent ions likely reduced artifacts introduced by simple elimination of Ca^{2+} . These control simulations showed that although the extracellular domain of C-cadherin partially retains its curved conformation on a 10-ns timescale

(Fig. 1, *E* and *F*), interrepeat motion was clearly enhanced and in some cases similar to that observed in the absence of Ca^{2+} (Fig. 3). Neither K^+ nor Na^+ ions seemed to maintain the rigidity of the C-cadherin extracellular domain. Furthermore, unbinding of both types of ions was observed throughout the simulations. Current limitations in the time-scale of MD simulations and the accuracy of force fields would likely prevent a quantitative characterization of the cadherin binding sites' selectivity, especially when comparing more subtle effects arising from the use of two different types of divalent ions. Thus, we refrained from performing further simulations in which Ca^{2+} is replaced by another divalent ion (such as Mg^{2+}).

Root mean-square deviations (RMSD), computed for individual repeats during SimCa1, SimApo1, SimK1, and SimNa1 (see Data S1, Fig. S10), reached stable values below 0.3 nm in all cases except one, indicating that individual repeats maintained their secondary structure on a nanosecond timescale even in the absence of Ca^{2+} . Repeat EC5 exhibited large RMSD values (>0.3 nm) during a simulation in which Ca^{2+} was replaced by K^+ (SimK1), likely reflecting deformations induced by unbinding of this large monovalent ion. RMSD values for repeats EC1 and EC2 were found to be consistently smaller than those for other repeats in simulations with Ca^{2+} , K^+ , and Na^+ . The slight increase in RMSD observed when calcium was removed (SimApo1) suggests that EC1 and EC2 are the most sensitive to Ca^{2+} binding.

The outcome of our equilibrium simulations are in line with those presented by Cailliez and Lavery (40,41) (using a different force-field and simulation engine) for only two repeats of E-cadherin and agree well with previous experimental results indicating that Ca^{2+} rigidifies the extracellular cadherin domain (30–34). Although our simulations span a

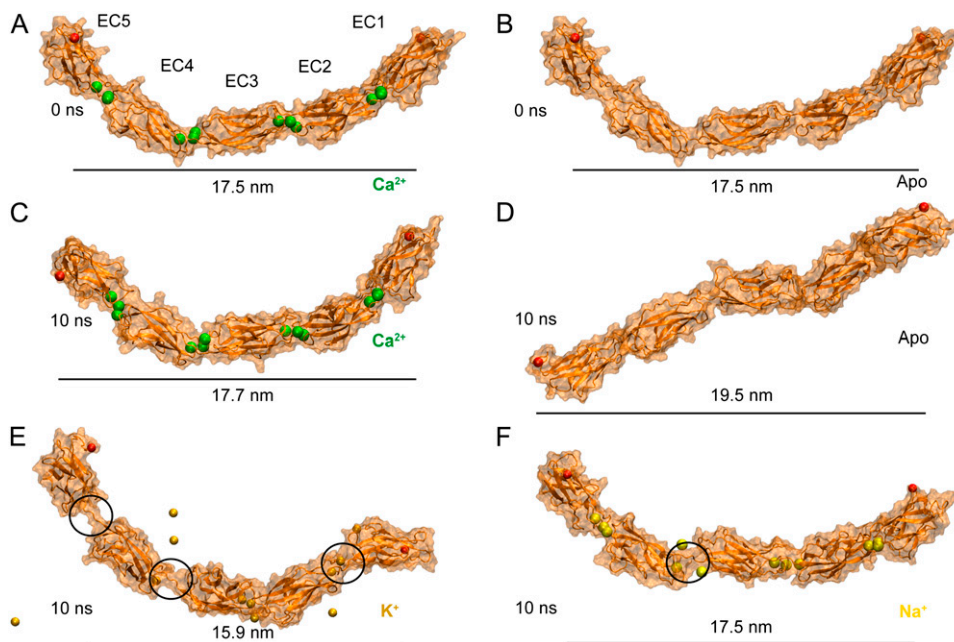


FIGURE 1 Influence of ions on C-cadherin equilibrium dynamics. (*A* and *B*) Models used as starting conformations in simulations of the complete C-cadherin extracellular domain with and without Ca^{2+} ions, respectively. The protein is shown in cartoon representation and its surface is drawn in transparent orange. Crystallographic Ca^{2+} and terminal C_α atoms are shown as green and red spheres. Water and bulk ions are not shown. (*C–F*) Snapshots of the complete extracellular domain of C-cadherin after 10 ns of equilibration in the presence of Ca^{2+} ions (SimCa1, *C*), in the absence of Ca^{2+} ions (SimApo1, *D*), with K^+ (SimK1, *E*), and with Na^+ ions (SimNa1, *F*), respectively. While C-cadherin remains curved when simulated in the presence of Ca^{2+} , its shape is lost after 10 ns of dynamics in the absence of Ca^{2+} . Both K^+ and Na^+ ions begin to unbind from C-cadherin during 10 ns of dynamics (black circles).

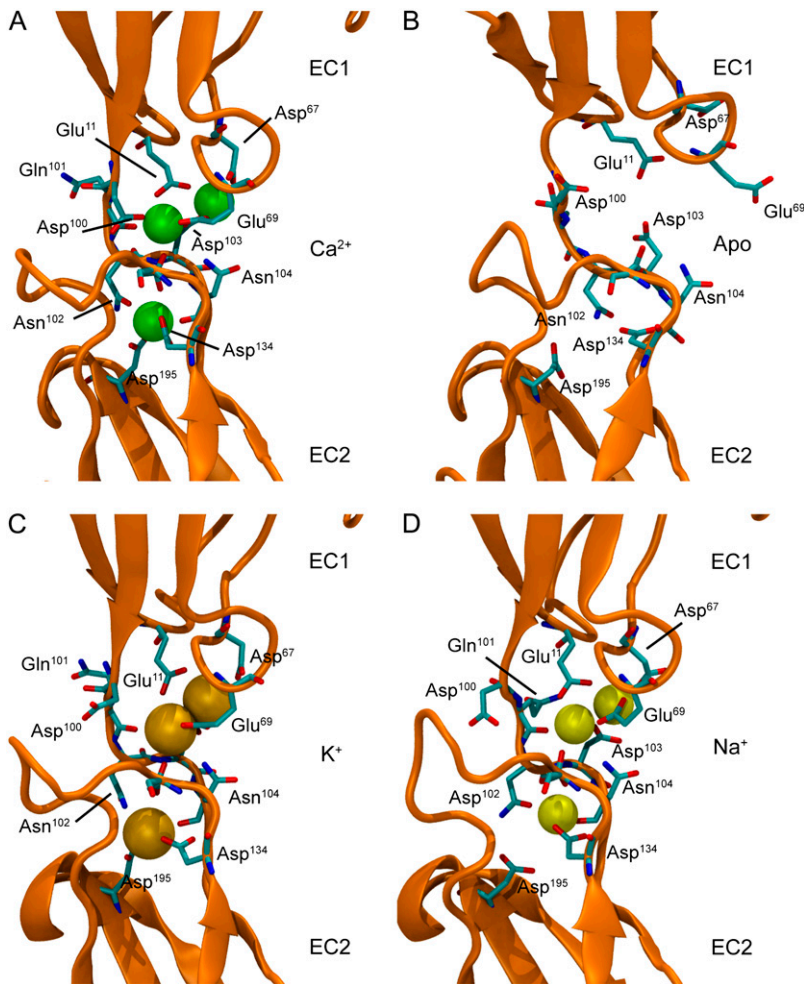


FIGURE 2 Linker region of C-cadherin repeats EC1-EC2. (A–D) Snapshots of the linker region between repeats EC1-EC2 of C-cadherin after 1.1 ns of simulation for systems with crystallographically resolved Ca^{2+} , without Ca^{2+} , with K^{+} , and with Na^{+} ions, respectively. The protein is shown in orange cartoon representation and ions are shown as green (Ca^{2+}), dark yellow (K^{+}), and light yellow (Na^{+}) spheres. Residues originally involved in Ca^{2+} binding are labeled and shown for all snapshots in licorice representation.

short timescale which precludes observation of a full collapse of cadherin repeats (as seen in electron microscopy and AFM images (30,58)) or possible unfolding, the simulations permitted us to clearly see interrepeat motion that could lead to a collapsed conformation in the absence of Ca^{2+} (Fig. 3, and see [Data S1](#), Figs. S8 and S9).

Tertiary structure elasticity of C-cadherin

We further probed cadherin stability by using conformations from equilibrium simulations as the starting points for constant-velocity steered molecular dynamics simulations (59–63). The SMD simulations were performed on systems with and without Ca^{2+} ions and on a system in which Na^{+} replaced the crystallographically resolved Ca^{2+} . Our SMD setup was similar to that used in Gräter et al. (64) as we attached both ends of the protein (C_{α}^1 and C_{α}^{540}) to virtual springs ($k_s = 1 \text{ kcal/mol/\text{Å}^2}$). The free ends of the springs moved in opposite directions at a constant velocity along the axis defined by the vector joining the protein termini. Different temperature control protocols and stretching velocities were utilized.

The SMD simulations revealed that upon stretching, the complete C-cadherin extracellular domain becomes straight by rearranging the relative orientation of individual repeats with respect to each other (see Fig. 4, *B* and *E*). This so-called tertiary structure elasticity (TSE) demonstrated earlier in other protein systems (39,63,65) was observed here in SMD simulations of C-cadherin with and without Ca^{2+} , and with Na^{+} replacing Ca^{2+} . While the apo SMD simulation shows that the linkers between repeats extend fairly easily in this case, the simulation with Ca^{2+} reveals that these ions act as molecular bearings, such that linker regions behave as stiff hinges and the extracellular domain responds as one unit.

We ask then whether cadherin's TSE is reversible. We turned off the applied forces at the end of simulations SimCa2 and SimApo2, and continued with equilibrium dynamics in two simulations labeled SimCa3 and SimApo3 lasting 10 ns and 5 ns, respectively. In both cases the protein relaxed and the end-to-end distance partially recovered the value observed before stretching (see Fig. 4, *C* and *F*, and see [Data S1](#), Fig. S11 A). However, while C-cadherin partially recovered curvature in the presence of Ca^{2+} (SimCa3, see Fig. 4 *C*), in the absence of Ca^{2+} (SimApo3) it relaxed into a conformation

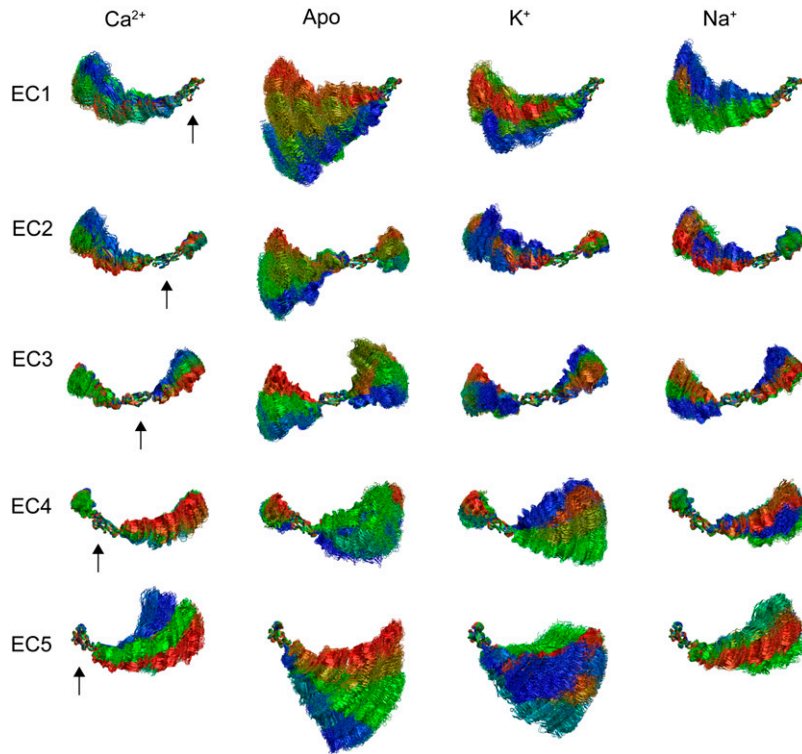


FIGURE 3 C-Cadherin equilibrium dynamics and influence of ions on interrepeat motion. Conformations of the extracellular domain of C-cadherin during simulations SimCa1, SimApo1, SimK1, and SimNa1 (lasting 10 ns each) were aligned so as to illustrate the relative motion of individual repeats with respect to their neighbors. Individual repeats (EC1–EC5 as indicated by *arrows*) were aligned throughout the trajectories using the crystal conformation as a reference. The rest of the protein was moved using the same matrix transformation required to align the corresponding repeat. The resulting aligned molecules are shown superimposed every 40 ps. Color indicates time, with red being early stages of the simulations and blue indicating the latest stages of the simulations. Interrepeat motion is readily observed in the absence of Ca^{2+} and when K^+ replaces Ca^{2+} . Even in the presence of Ca^{2+} the extracellular domain of C-cadherin is not completely rigid, as suggested by limited but significant interrepeat motion (particularly for repeat EC5).

even more disordered than the one observed before stretching (disorder meaning that relative orientation of individual repeats was not uniform as seen in Fig. 4 *F* and in [Movie S1](#), movies mI and mII; and [Data S1](#), Fig. S12). Reversibility for the Apo simulation arises only in regard to end-to-end distance, as confirmed by the RMSD of the complete structure computed during stretching and relaxation (see [Data S1](#), Fig.

S11 *B*). The latter result suggests that TSE has different molecular origins in both cases. Interestingly, RMSD of individual repeats remained below 0.3 nm throughout the whole stretching and relaxation trajectories in the presence and the absence of calcium, confirming that linkers are responsible for the observed shape changes. Furthermore, partial recovery of C-cadherin's shape in the presence of

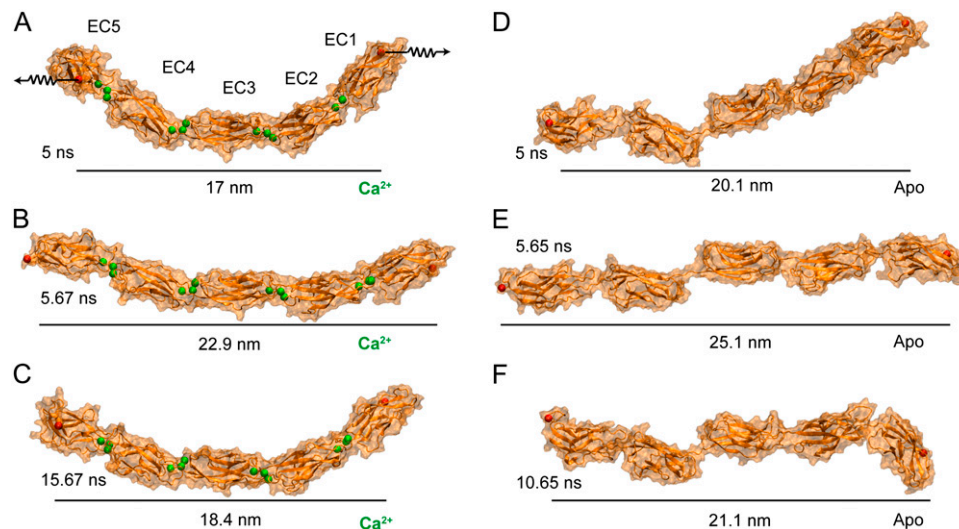


FIGURE 4 C-Cadherin tertiary structure elasticity. (*A–C*) Snapshots of the complete extracellular domain of C-cadherin simulated in the presence of Ca^{2+} ions after 5 ns of equilibration (SimCa1), after 0.67 ns of a constant velocity stretching (SimCa2), and after 10 ns of a subsequent relaxation (SimCa3), respectively. The protein is shown in cartoon representation and its surface is drawn in transparent orange. Crystallographic Ca^{2+} and termini Ca_α atoms are shown as green and red spheres, respectively. (*D–F*) Snapshots of the C-cadherin extracellular domain simulated in the absence of Ca^{2+} after 5 ns of equilibration (SimApo1), after 0.65 ns of constant velocity stretching (SimApo2), and after 5 ns of a subsequent relaxation (SimApo3), respectively. The extracellular domain of C-cadherin exhibits limited flexibility in the presence of Ca^{2+} and independent interrepeat mobility in the absence of Ca^{2+} .

divalent ions suggests that its curvature is not an artifact caused by crystallographic packing.

Local deformations of the C-cadherin structure were also monitored by computing the average strain per residue (see Methods and (56)) during equilibration, short stretching, and relaxation simulations in the presence and absence of Ca^{2+} (see [Movie S1](#), movies mIII and mIV). In the presence of Ca^{2+} , the largest strains were observed in loops of repeats EC3, EC4, and EC5 and the corresponding linker regions. In the absence of Ca^{2+} , the largest strains were observed in all linker regions and loops, confirming once again the role of Ca^{2+} ions in interrepeat motion and TSE.

Tertiary structure elasticity was first predicted through simulations of the protein Ankyrin-R (9,39), and subsequently confirmed through AFM experiments involving Ankyrin-B (66). Both ankyrin proteins feature 24 repeat units but, unlike cadherin, ankyrin repeats interact with each other through extensive hydrophobic surfaces, the parallel stack of repeats forming a curved superhelical arrangement (67). The reversible, nonentropic TSE observed for ankyrin resembles better the one observed here for cadherin with calcium ions, while the TSE observed for cadherin without ions seems to be rather entropic in origin, although some residual interactions at the linkers may remain. Whether such difference in the origin of the observed TSE can be distinguished through experimental force spectroscopy or if it is relevant at all for adhesion are questions that remain to be answered. However, a simple calculation can set some limits for the elasticity in both cases. A freely jointed chain with n segments of length b each would exhibit an entropic spring constant of $k = (3k_B T/nb^2) \sim 0.1 \text{ mN/m}$ (lower limit of k for cadherin without Ca^{2+} at low force using $n = 5$ and $b = 5 \text{ nm}$), while a straight rigid rod 23 nm (L) long and 2 nm ($2r$) wide would exhibit a longitudinal stiffness of $k = (E\pi r^2/L) \sim 270 \text{ mN/m}$ (upper limit of k for cadherin with Ca^{2+} using a Young's modulus for collagen of $E = 2 \text{ GPa}$).

A rough estimate of the elastic constant of C-cadherin with and without Ca^{2+} was obtained using a novel SMD protocol termed “length-clamp” (SimCa13/SimCa17 and SimApo9; see Methods and [Data S1](#), Fig. S13). The estimated spring constants from elastic forces (68), $k_{\text{Ca}^{2+}} \sim 50 \text{ mN/m}$ (400/8 pN/nm) and $k_{\text{Apo}} \sim 25 \text{ mN/m}$ (200/8 pN/nm), are within the boundaries computed above. These simulations also reveal that the complete C-cadherin extracellular domain exhibits a viscoelastic behavior.

Secondary structure elasticity of C-cadherin

The simulations described above depict the extracellular domain of cadherin switching from a rodlike to a flexible-chain-like behavior upon removal of Ca^{2+} at low force regimes. While unfolding of individual domains may not play a physiological role in adhesion (44), we explored the effect of calcium and sodium on the stability of individual domains when subject to large forces inducing mechanical unfolding. Two SMD simulations (SimCa2 and SimApo2) were further continued until stretching forces unfolded one repeat (SimCa2E and SimApo2E) and eight new SMD simulations (SimCa5, SimCa6, SimCa7, SimCa8, SimCa9, SimApo6, SimApo7, and SimApo8) were performed using different steering velocities and thermodynamic ensemble protocols.

The SMD simulations showed what is perhaps the most dramatic difference between the elastic response of the protein with or without Ca^{2+} . While the EC1 repeat unfolded fairly easily in the absence of Ca^{2+} (see Fig. 5 A), unfolding of EC1 in the presence of Ca^{2+} required a considerably larger force (1664 pN compared to 858 pN at $v = 10 \text{ nm/ns}$) that breaks a bond between residue Glu¹¹ and a Ca^{2+} ion (Fig. 5, B–E, and see [Data S1](#), Figs. S14 and S15, and [Movie S1](#) and [Movie S2](#), movies mV–mVII). Peak forces arising in a SMD simulation unfolding cadherin in which Ca^{2+} ions were replaced by Na^+ (SimNa) were only slightly larger than those

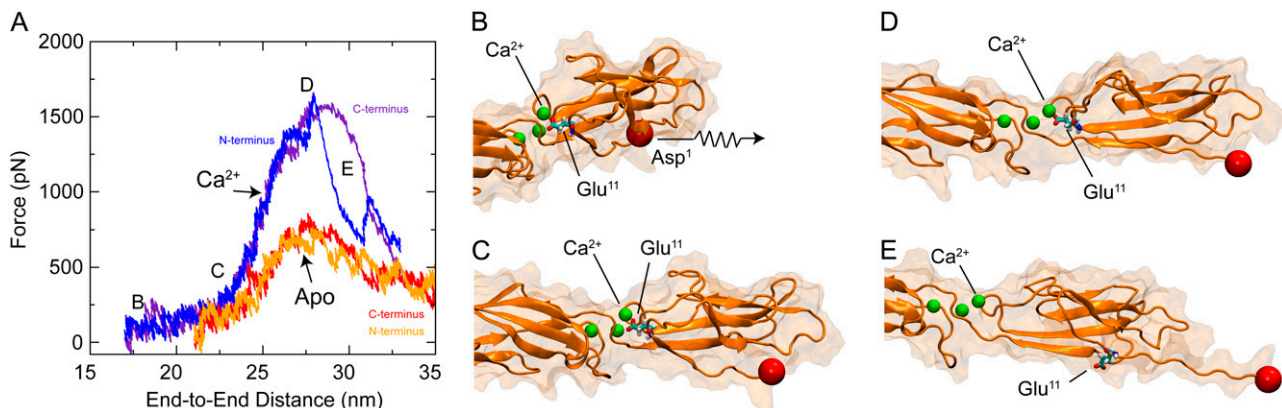


FIGURE 5 C-Cadherin secondary structure elasticity. (A) Force versus end-to-end distance profile for constant-velocity stretching simulations with crystallographic Ca^{2+} ions (blue and indigo, SimCa2-SimCa2E) and without Ca^{2+} (red and orange, SimApo2-SimApo2E). (B–E) Snapshots of the unfolding pathway during simulation SimCa2E. Views show the EC1-linker-EC2 domain in cartoon representation with the corresponding surface drawn in transparent orange. The C_α atom of the N-terminus is shown as a red sphere and Ca^{2+} ions as green spheres. Residue Glu¹¹ is shown in licorice representation. Disruption of secondary structure elements (secondary structure elasticity) proceeds only upon rupture of a bridge formed by Glu¹¹ and a Ca^{2+} ion.

observed for the simulations performed in the absence of Ca^{2+} , reinforcing the relevance of Ca^{2+} for the stability of C-cadherin (see [Data S1](#), Fig. S16).

Additional simulations performed at different stretching speeds (SimCa7, SimCa8, SimCa9, and SimApo8 in Table 1) confirmed a similar unfolding scenario and a reduction in unfolding force peaks upon decrease of v , as expected (69,70) (see [Data S1](#), Fig. S17). It remains to be elucidated whether the difference observed in peak forces for C-cadherin between simulations with and without Ca^{2+} is as dramatic at slow pulling speeds as it is at the speeds used in this study. Even the slowest stretching velocity used in our SMD simulations is large compared to those used in AFM or other experimental techniques (1 nm/ns vs. 10^{-5} nm/ns), since all-atom molecular dynamics simulations can usually achieve only a submicrosecond timescale. Despite this limitation, multiple SMD studies, all similarly exceeding experimental pulling speeds, have provided qualitative and quantitative predictions confirmed by experiments (39,63,71–77).

The SMD simulations mentioned above were performed in the NVE ensemble. Further simulations performed in the NpT ensemble (SimCa5, SimCa6, SimApo6, SimApo7) confirmed the Ca^{2+} -dependent mechanical stability of the C-cadherin domain. However, even when using a small damping coefficient, Langevin dynamics (NpT) resulted in an artificial increase of unfolding peak forces and, in the worst case, complete decoupling of forces measured at opposite ends of the protein (see [Data S1](#), Fig. S18).

Unfolding forces for EC1 in all cases are considerably smaller than the forces required to unfold a single EC2 repeat simulated under similar conditions but isolated from the rest of the structure (reported in our earlier SMD simulations (39)). The results are consistent with temperature- and denaturant-induced unfolding experiments of E-cadherin showing that Ca^{2+} stabilizes cadherin repeats and that EC1 is weaker than EC2 (36). However, the mechanical unfolding of the EC2 repeat within the entire C-cadherin extracellular domain may differ from that of the isolated repeat. We therefore probed the mechanical response of repeats EC2 and EC4 by steering the center-of-mass of repeats EC3/EC1 and repeats EC5/EC3 in opposite directions (effectively stretching repeats EC2 and EC4, see [Data S1](#), Fig. S19 A). The simulations (SimCa10 and SimCa11) revealed that the EC4-EC5 linker is weaker than the EC1-EC2 linker, indicating a possible mechanical hierarchy for cadherin repeats/linkers. Interestingly, the unfolding force for repeat EC2 within the complete domain is comparable to that of the isolated repeat (see [Data S1](#), Fig. S19 B), and both unfolding pathways exhibit an intermediate state in which the repeat is partially unfolded due to rupture of interactions between conserved residues and Ca^{2+} ions. Such a state may be particularly relevant under physiological conditions, as it provides a safety mechanism in which cadherin can extend in response to sustained mechanical stimuli and easily refold when the external force is turned off.

Previous SMD simulations identified two types of mechanical unfolding processes for immunoglobulin-like domains (78) in which water mediates rupture of hydrogen bonds concertedly (sheering mode) or one-by-one (zipper mode). In both types of unfolding, rupture of hydrogen bonds between β -strands (concertedly or one-by-one) gives rise to the unfolding force-peak. Based on the results presented here and in Sotomayor et al. (39), we add a third mechanical unfolding category in which a bridge between charged amino acids and divalent ions produces the unfolding force-peak. Thus, Ca^{2+} is not only acting as a molecular bearing that facilitates cooperative motion of cadherin repeats, but also as a staple that maintains the stability of the structure providing further resistance to mechanical unfolding.

Unfolding as observed with the SMD methodology employed here permitted us to also estimate a characteristic time for stress propagation through the protein. This example shows how an unfolding event that occurred at one end of a protein is perceived at the other end (by the second steering spring considered now as a sensor) after some time. The force peaks measured through spring extension at both ends of the protein are not synchronous (see [Data S1](#), Fig. S14). In fact, in SimCa2E, a delay between the appearances of force peaks at both ends of the protein can be used to compute a velocity $v \sim 285 \text{ \AA}/38 \text{ ps} \sim 747 \text{ m/s}$ at the corresponding extension of the protein. This velocity may depend on multiple factors including the thermodynamic ensemble used in the simulation, stretching velocity, spring constants used for stretching springs, and criteria used to determine the characteristic time. Indeed, our simulations show that damping artificially introduced by temperature control algorithms may decouple different zones of the protein from each other (see [Data S1](#), Fig. S18). Although protein motions are largely overdamped (79), it has been hypothesized that stress signals could propagate over large distances in the cell (80). The two-end stretching approach outlined here may serve to test this hypothesis experimentally and theoretically.

Ca^{2+} allosteric control of residues involved in cell adhesion

The dynamics of the extracellular domain, controlled by Ca^{2+} , determines the availability of repeat EC1 to form adhesive contacts with proteins coming from neighboring cells. There are also subtle changes in C-cadherin dynamics controlled by Ca^{2+} that will affect its adhesive properties. For instance, we monitored the dynamics of the conserved residue Trp² throughout equilibrium simulations in presence and absence of Ca^{2+} , as well as with K^+ and Na^+ replacing Ca^{2+} . As mentioned above, Trp² is thought to mediate *trans*-interactions of cadherin by inserting itself in a hydrophobic pocket of another EC1 repeat coming from either the same cell or an adjacent cell (*cis* versus *trans*). The conformation of Trp² in the C-cadherin structure is that of an exposed residue (see first snapshot in Fig. 6 E), since the crystallographic

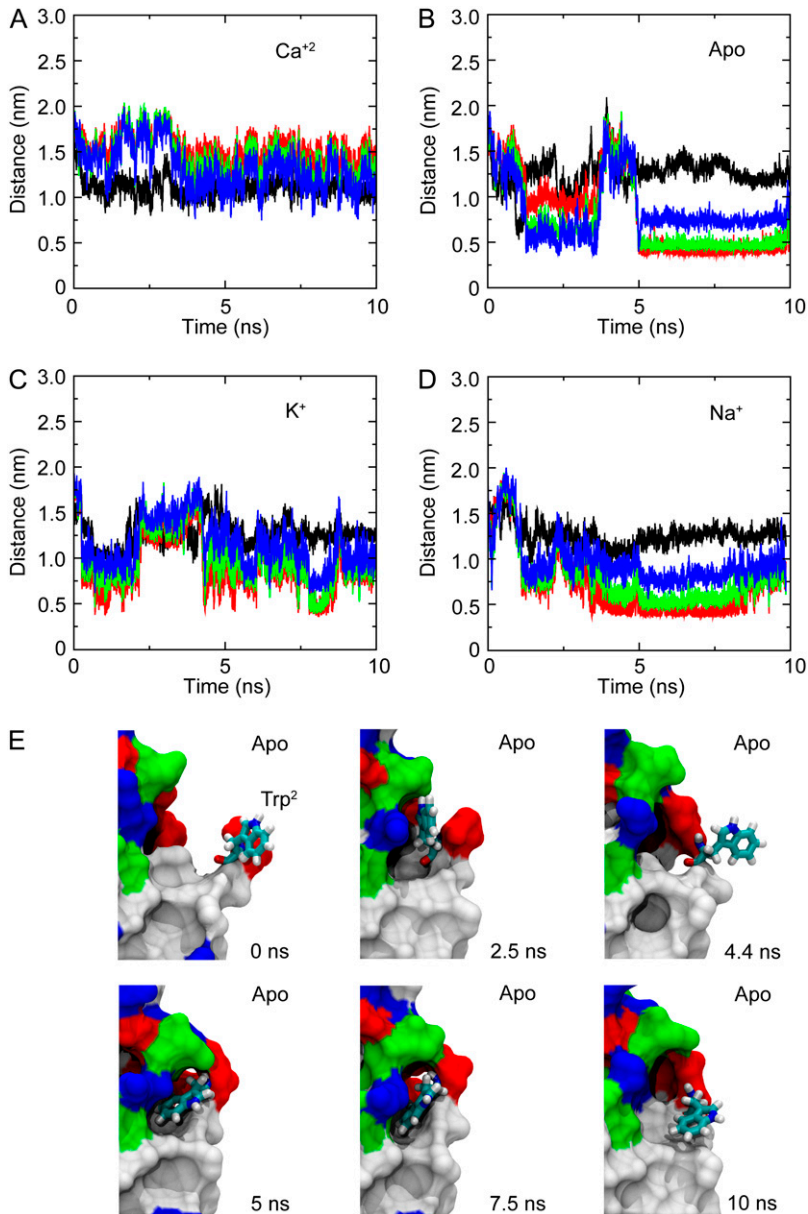


FIGURE 6 Dynamics of Trp². The state of Trp² is characterized by the distance to its neighboring residues during simulations with (A) and without (B) Ca²⁺, as well as with K⁺ (C) and Na⁺ (D) ions replacing Ca²⁺. Distances between the C α atom of Trp² and C α atoms of residues Ile²⁴, Lys²⁵, and Ser²⁶ are shown in red, green, and blue, respectively. The distance between atom N ϵ of Trp² and the carbonyl oxygen atom of Glu⁹⁰ is shown in black. Intermittent bound states can be clearly observed during simulations performed without Ca²⁺. (E) Snapshots show Trp² in licorice representation at times $t = 0, 2.5, 4.4, 5, 7.5,$ and 10 ns during SimApo1. The rest of the EC1 domain is shown in surface representation and colored according to hydrophobicity (white, hydrophobic residues; green, polar residues; red or blue, charged residues).

arrangement of the cadherin molecule leads to a proposed *trans* interaction (strand-exchanged) between molecules of different crystallographic unit cells. During the simulations in which calcium ions were present (SimCa1, SimCa3, and SimCa4), the side chain of Trp² remained partially exposed at all times (Fig. 6 A and see Data S1, Fig. S20 A). However, when calcium ions were removed or replaced by monovalent ions, the EC1 domain was more mobile (see root mean-square fluctuations in Data S1, Fig. S21 A) and the side chain of Trp² fluctuated between two states: exposed, and partially buried (see Fig. 7, snapshots in Fig. 6 E, and see Data S1, Fig. S20, B and C, and Movie S2, movies mVIII–mXI). In the latter state, the side chain is hidden in a hydrophobic pocket (intramolecular docking), close to residues 24 and 25. We termed this state partially buried since interactions

with E90 (D90 in E-cadherin) seen in other structures and NMR experiments with E-cadherin are not observed here, perhaps due to the short timescale of the simulation. The solvent-accessible surface area for Trp² computed throughout different equilibrium simulations also confirms the greater availability of this side chain when Ca²⁺ is bound to C-cadherin (see Data S1, Fig. S22). Our results strongly support experimental work using antibodies and independent mutagenesis experiments combined with force measurements suggesting that Trp² availability is allosterically modulated by Ca²⁺ (38,45).

The dynamic switching of Trp² availability is also compatible with the strand-exchanged adhesive interface (81), as backbone atoms of residues 25 and 27 (involved in hydrogen bonds with backbone atoms of residues 1 and 3 of a neigh-

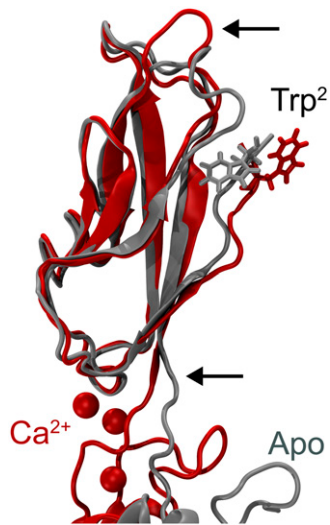


FIGURE 7 Allosteric switch of Trp². Snapshots of C-cadherin repeat EC1 and EC1-EC2 linker region at the end of SimCa1 (red) and after 5 ns of dynamics in SimApo1 (gray) are superimposed and shown in cartoon representation. Calcium ions are shown as spheres. The two conformations adopted by Trp² are evident. Arrows indicate regions of the protein backbone where significant differences between the two conformations can be observed.

boring molecule) are more exposed when Ca²⁺ is present and the Trp² side chain is in its extended conformation. The Trp² side chain may directly and indirectly mediate the formation of the strand-exchanged interface. Interestingly, the behavior observed here for Trp² is similar to that observed for a Trp^{185/187} residue in rat/human Annexin V, where Ca²⁺ induces exposure of the Trp side chain (involved in membrane-protein interactions) (82,83), thus hinting at a more general mechanism behind calcium-mediated adhesion.

DISCUSSION

The results presented here qualitatively validate molecular dynamics simulations as a tool to study the mechanical function of cadherin. The simulations, using standard and widely used parameters, account for experimentally known facts such as the role of Ca²⁺ in shaping the extracellular cadherin domain, the putative allosteric effect of Ca²⁺ on the key binding residue Trp², and the Ca²⁺-dependent stability of individual repeats probed here through mechanical unfolding. At the same time, the simulations provide a unique atomistic view of cadherin dynamics. Such a detailed view is a necessary complement to experiments investigating cadherin function.

The reversible TSE observed here for C-cadherin provides support for the multiple conformations observed in desmosomal cadherins through electron tomography (84) and also suggest that the extracellular domains of cadherin molecules should not be considered as completely rigid units, even in the presence of Ca²⁺. Moreover, the allosteric control of Trp² conformations by Ca²⁺ observed, to the best of our knowl-

edge, for the first time at the atomic level in our simulations, provides a conceptual framework to interpret mutations that modify sites located far from the strand-exchanged adhesive interface (81) but may allosterically affect residues involved in adhesion as well as binding selectivity.

This study serves as a step toward future molecular dynamics studies of cadherin that should address:

1. The relevance of cadherin elasticity and mechanical intermediates for adhesion;
2. The robustness of the intrinsic curvature of C-cadherin in response to multiple stretching and compressing cycles;
3. The mechanical stability and complete unfolding of all repeats;
4. The selectivity of adhesion molecules (85,86) in the complete adhesion complex; and, eventually,
5. The mechanical or allosteric role of mutations affecting calcium binding sites in cadherin-23 and protocadherin-15 resulting in hereditary deafness (12,87,88).

Our simulations strongly suggest that deafness may arise through mutations that affect the cadherin-23/protocadherin-15 hair-cell tip link in two ways: abolishing tip-link formation by directly or allosterically interfering with residues involved in adhesion or dimerization; and/or by modifying the mechanical strength of the tip link by favoring unfolding or precluding mechanical intermediates by breaking bridges between protein atoms and Ca²⁺ ions at linker regions.

The results presented here have implications for other proteins featuring tandemly-arranged repeats, the archetypical examples being spectrin and titin. Linkers have been shown to be important in spectrin elasticity (56,89,90), while interdomain motion and divalent ions may likely play a role in titin elasticity (91). Cadherin may serve as an exceptional example of the design principles behind linker-mediated elasticity, as it features unique linker regions that can behave as stiff or flexible hinges, depending on the availability of calcium ions.

SUPPLEMENTARY MATERIAL

To view all of the supplemental files associated with this article, visit www.biophysj.org.

We thank Deborah Leckband, Alek Aksimentiev, David P. Corey, Bechara Kachar, and members of the Theoretical and Computational Biophysics Group for helpful discussions. The molecular images in this article were created with the molecular graphics program VMD.

This work was supported by funds from the National Institutes of Health (grants No. P41 RR05969 and No. 1 R01 GM073655). The authors also acknowledge computer time provided by the National Science Foundation through LRAC grant No. MCA93S028.

REFERENCES

1. Takeichi, M. 1990. Cadherins: a molecular family important in selective cell-cell adhesion. *Annu. Rev. Biochem.* 59:237–252.

2. Hynes, R. O. 1999. Cell adhesion: old and new questions. *Trends Cell Biol.* 9:M33–M37.
3. Takeichi, M. 2005. Looking for cell-cell adhesion molecules: a cadherin story. *Proc. Jpn. Acad.* 81:321–328.
4. Gumbiner, B. M. 2005. Regulation of cadherin-mediated adhesion in morphogenesis. *Nat. Rev. Mol. Cell Biol.* 6:622–634.
5. Takeichi, M. 1991. Cadherin cell adhesion receptors as a morphogenetic regulator. *Science.* 251:1451–1455.
6. Takeichi, M. 1995. Morphogenetic roles of classic cadherins. *Curr. Opin. Cell Biol.* 7:619–627.
7. Takeichi, M. 2007. The cadherin superfamily in neuronal connections and interactions. *Nat. Rev. Neurosci.* 8:11–20.
8. Leckband, D., and A. Prakasam. 2006. Mechanism and dynamics of cadherin adhesion. *Annu. Rev. Biomed. Eng.* 8:259–287.
9. Corey, D. P., and M. Sotomayor. 2004. Tightrope act. *Nature.* 428:901–902.
10. Söllner, C., G.-J. Rauch, J. Siemens, R. Geisler, S. C. Schuster, U. Müller, and T. Nicolson. 2004. The Tübingen 2000 Screen Consortium. Mutations in cadherin 23 affect tip links in zebrafish sensory hair cells. *Nature.* 428:955–958.
11. Siemens, J., C. Lillo, R. A. Dumont, A. Reynolds, D. S. Williams, P. G. Gillespie, and U. Müller. 2004. Cadherin 23 is a component of the tip link in hair-cell stereocilia. *Nature.* 428:950–955.
12. Kazmierczak, P., H. Sakaguchi, J. Tokita, E. M. Wilson-Kubalek, R. A. Milligan, U. Müller, and B. Kachar. 2007. Cadherin 23 and protocadherin 15 interact to form tip-link filaments in sensory hair cells. *Nature.* 449:87–91.
13. Shapiro, L., P. D. Kwong, A. M. Fannon, D. R. Colman, and W. A. Hendrickson. 1995. Consideration on the folding topology and evolutionary origin of cadherin domains. *Proc. Natl. Acad. Sci. USA.* 92:6793–6797.
14. Nollet, F., P. Kools, and F. van Roy. 2000. Phylogenetic analysis of the cadherin superfamily allows identification of six major subfamilies besides several solitary members. *J. Mol. Biol.* 299:551–572.
15. Patel, S. D., C. P. Chen, F. Bahna, B. Honig, and L. Shapiro. 2003. Cadherin-mediated cell-cell adhesion: sticking together as a family. *Curr. Opin. Struct. Biol.* 13:690–698.
16. Koch, A. W., D. Bozi, O. Pertz, and J. Engel. 1999. Homophilic adhesion by cadherins. *Curr. Opin. Struct. Biol.* 9:275–281.
17. Nagar, B., M. Overdulin, M. Ikura, and J. Rini. 1996. Structural basis of calcium-induced E-cadherin rigidification and dimerization. *Nature.* 380:360–364.
18. Tomschy, A., C. Fauser, R. Landwehr, and J. Engel. 1996. Homophilic adhesion of E-cadherin occurs by a co-operative two-step interaction of N-terminal domains. *EMBO J.* 15:3507–3514.
19. Yap, A. S., W. M. Briehar, M. Pruschy, and B. M. Gumbiner. 1997. Lateral clustering of the adhesive ectodomain: a fundamental determinant of cadherin function. *Curr. Biol.* 7:308–315.
20. Takeda, H., Y. Shimoyama, A. Nagafuchi, and S. Hirohashi. 1999. E-cadherin functions as a cis-dimer at the cell-cell adhesive interface *in vivo*. *Nat. Struct. Biol.* 6:310–312.
21. Klingelhöfer, J., O. Y. Laur, R. B. Troyanovsky, and S. M. Troyanovsky. 2002. Dynamic interplay between adhesive and lateral E-cadherin dimers. *Mol. Cell Biol.* 22:7449–7458.
22. Ahrens, T., M. Lambert, O. Pertz, T. Sasaki, T. Schulthess, R.-M. Mège, R. Timpl, and J. Engel. 2003. Homoassociation of VE-cadherin follows a mechanism common to “classical” cadherins. *J. Mol. Biol.* 325:733–742.
23. Sivasankar, S., W. Briehar, N. Lavrik, B. Gumbiner, and D. Leckband. 1999. Direct molecular force measurements of multiple adhesive interactions between cadherin ectodomains. *Proc. Natl. Acad. Sci. USA.* 96:11820–11824.
24. Sivasankar, S., B. Gumbiner, and D. Leckband. 2001. Direct measurements of multiple adhesive alignments and unbinding trajectories between cadherin extracellular domains. *Biophys. J.* 80:1758–1768.
25. Chappuis-Flament, S., E. Wong, L. D. Hicks, C. M. Kay, and B. M. Gumbiner. 2001. Multiple cadherin extracellular repeats mediate homophilic binding and adhesion. *J. Cell Biol.* 154:231–243.
26. Zhu, B., S. Chappuis-Flament, E. Wong, I. E. Jensen, B. M. Gumbiner, and D. Leckband. 2003. Functional analysis of the structural basis of homophilic cadherin adhesion. *Biophys. J.* 84:4033–4042.
27. Perret, E., A. Leung, and E. Evans. 2004. Trans-bonded pairs of E-cadherin exhibit a remarkable hierarchy of mechanical strengths. *Proc. Natl. Acad. Sci. USA.* 101:16472–16477.
28. Bayas, M. V., A. Leung, E. Evans, and D. Leckband. 2006. Lifetime measurements reveal kinetic differences between homophilic cadherin bonds. *Biophys. J.* 90:1385–1395.
29. Tsukasaki, Y., K. Kitamura, K. Shimizu, A. H. Iwane, Y. Takai, and T. Yanagida. 2007. Role of multiple bonds between the single cell adhesion molecules, nectin and cadherin, revealed by high sensitive force measurements. *J. Mol. Biol.* 367:996–1006.
30. Pokutta, K., S. Herrenknecht, R. Kemler, and J. Engel. 1994. Conformational changes of the recombinant extracellular domain of E-cadherin upon calcium binding. *Eur. J. Biochem.* 223:1019–1026.
31. Alattia, J.-R., J. B. Ames, T. Porumb, K. I. Tong, Y. M. Heng, P. Ottensmeyer, C. M. Kay, and M. Ikura. 1997. Lateral self-assembly of E-cadherin directed by cooperative calcium binding. *FEBS Lett.* 417:405–408.
32. Koch, A. W., S. Pokutta, A. Lustig, and J. Engel. 1997. Calcium binding and homoassociation of E-cadherin domains. *Biochemistry.* 36:7696–7705.
33. Pertz, O., D. Bozic, A. W. Koch, C. Fauser, A. Brancaccio, and J. Engel. 1999. A new crystal structure, Ca²⁺ dependence and mutational analysis reveal molecular details of E-cadherin homoassociation. *EMBO J.* 18:1738–1747.
34. Häussinger, D., T. Ahrens, H.-J. Sass, O. Pertz, J. Engel, and S. Grzesiek. 2002. Calcium-dependent homoassociation of E-cadherin by NMR spectroscopy: changes in mobility, conformation and mapping of contact regions. *J. Mol. Biol.* 324:823–839.
35. Boggon, T. J., J. Murray, S. Chappuis-Flament, E. Wong, B. M. Gumbiner, and L. Shapiro. 2002. C-cadherin ectodomain structure and implications for cell adhesion mechanisms. *Science.* 296:1308–1313.
36. Prasad, A., and S. Pedigo. 2005. Calcium-dependent stability studies of domains 1 and 2 of epithelial cadherin. *Biochemistry.* 44:13692–13701.
37. Prasad, A., H. Zhao, J. M. Rutherford, H. N. C. Nichols, and S. Pedigo. 2006. Effect of linker segments on the stability of epithelial cadherin domain 2. *Proteins Struct. Funct. Bioinform.* 62:111–121.
38. Prakasam, A., Y.-H. Chien, V. Maruthamuthu, and D. E. Leckband. 2006. Calcium site mutations in cadherin: impact on adhesion and evidence of cooperativity. *Biochemistry.* 45:6930–6939.
39. Sotomayor, M., D. P. Corey, and K. Schulten. 2005. In search of the hair-cell gating spring: elastic properties of ankyrin and cadherin repeats. *Structure.* 13:669–682.
40. Cailliez, F., and R. Lavery. 2005. Cadherin mechanics and complexation: the importance of calcium binding. *Biophys. J.* 89:3895–3903.
41. Cailliez, F., and R. Lavery. 2006. Dynamics and stability of E-cadherin dimers. *Biophys. J.* 91:3964–3971.
42. Shapiro, L., A. M. Fannon, P. D. Kwong, A. Thompson, M. S. Lehmann, G. Grübel, J. F. Legrand, J. Als-Nielsen, D. R. Colman, and W. A. Hendrickson. 1995. Structural basis of cell-cell adhesion by cadherins. *Nature.* 374:327–336.
43. Häussinger, D., T. Ahrens, T. Aberle, J. Engel, J. Stetefeld, and S. Grzesiek. 2004. Proteolytic E-cadherin activation followed by solution NMR and x-ray crystallography. *EMBO J.* 23:1699–1708.
44. Bayas, M. V., K. Schulten, and D. Leckband. 2004. Forced dissociation of the strand dimer interface between C-cadherin ectodomains. *Mech. Chem. Biosystems.* 1:101–111.
45. Harrison, O. J., E. M. Corps, T. Berge, and P. J. Kilshaw. 2005. The mechanism of cell adhesion by classical cadherins: the role of domain 1. *J. Cell Sci.* 118:711–721.

46. Humphrey, W., A. Dalke, and K. Schulten. 1996. VMD—visual molecular dynamics. *J. Mol. Graph.* 14:33–38.
47. Phillips, J. C., R. Braun, W. Wang, J. Gumbart, E. Tajkhorshid, E. Villa, C. Chipot, R. D. Skeel, L. Kale, and K. Schulten. 2005. Scalable molecular dynamics with NAMD. *J. Comput. Chem.* 26:1781–1802.
48. MacKerell, A. D., Jr., D. Bashford, M. Bellott, J. R. L. Dunbrack, J. Evanseck, M. J. Field, S. Fischer, J. Gao, H. Guo, S. Ha, D. Joseph, L. Kuchnir, K. Kuczera, F. T. K. Lau, C. Mattos, S. Michnick, T. Ngo, D. T. Nguyen, B. Prodhom, B. Roux, M. Schlenkrich, J. Smith, R. Stote, J. Straub, M. Watanabe, J. Wiorkiewicz-Kuczera, D. Yin, and M. Karplus. 1992. Self-consistent parameterization of biomolecules for molecular modeling and condensed phase simulations. *FASEB J.* 6:A143.
49. MacKerell, A., Jr., D. Bashford, M. Bellott, R. L. Dunbrack, Jr., J. Evanseck, M. J. Field, S. Fischer, J. Gao, H. Guo, S. Ha, D. Joseph, L. Kuchnir, K. Kuczera, F. T. K. Lau, C. Mattos, S. Michnick, T. Ngo, D. T. Nguyen, B. Prodhom, I. W. E. Reiher, B. Roux, M. Schlenkrich, J. Smith, R. Stote, J. Straub, M. Watanabe, J. Wiorkiewicz-Kuczera, D. Yin, and M. Karplus. 1998. All-atom empirical potential for molecular modeling and dynamics studies of proteins. *J. Phys. Chem. B.* 102:3586–3616.
50. MacKerell, A. D., M. Feig, and C. L. Brooks III. 2004. Extending the treatment of backbone energetics in protein force fields: limitations of gas-phase quantum mechanics in reproducing protein conformational distributions in molecular dynamics simulations. *J. Comput. Chem.* 25:1400–1415.
51. Young, A., J. Dewan, C. Nave, and R. Tilton. 1993. Comparison of radiation-induced decay and structure refinement from x-ray data collected from lysozyme crystals at low and ambient temperatures. *J. Appl. Cryst.* 26:309–319.
52. Buck, M., S. Bouguet-Bonnet, R. W. Pastor, and A. D. MacKerell. 2006. Importance of the CMAP correction to the CHARMM22 protein force field: dynamics of hen lysozyme. *Biophys. J.* 90:L36–L38.
53. Jorgensen, W. L., J. Chandrasekhar, J. D. Madura, R. W. Impey, and M. L. Klein. 1983. Comparison of simple potential functions for simulating liquid water. *J. Chem. Phys.* 79:926–935.
54. Marchand, S., and B. Roux. 1998. Molecular dynamics study of calbindin D_{9k} in the apo and singly and doubly calcium-loaded states. *Proteins Struct. Funct. Genet.* 33:265–284.
55. Essmann, U., L. Perera, M. L. Berkowitz, T. Darden, H. Lee, and L. G. Pedersen. 1995. A smooth particle mesh Ewald method. *J. Chem. Phys.* 103:8577–8593.
56. Ortiz, V., S. O. Nielsen, M. L. Klein, and D. E. Discher. 2005. Unfolding a linker between helical repeats. *J. Mol. Biol.* 349:638–647.
57. Zhong, Y., W. M. Briehner, and B. M. Gumbiner. 1999. Analysis of C-cadherin regulation during tissue morphogenesis with an activating antibody. *J. Cell Biol.* 144:351–359.
58. Baumgartner, W., P. Hinterdorfer, W. Ness, A. Raab, D. Vestweber, H. Schindler, and D. Drenckhahn. 2000. Cadherin interaction probed by atomic force microscopy. *Proc. Natl. Acad. Sci. USA.* 97:4005–4010.
59. Izrailev, S., S. Stepaniants, B. Isralewitz, D. Kosztin, H. Lu, F. Molnar, W. Wriggers, and K. Schulten. 1998. Steered molecular dynamics. In *Computational Molecular Dynamics: Challenges, Methods, Ideas*, Vol. 4 of Lecture Notes in Computational Science and Engineering. P. Deuffhard, J. Hermans, B. Leimkuhler, A. E. Mark, S. Reich, and R. D. Skeel, editors. Springer-Verlag, Berlin.
60. Isralewitz, B., J. Baudry, J. Gullingsrud, D. Kosztin, and K. Schulten. 2001. Steered molecular dynamics investigations of protein function. *J. Mol. Graphics Modeling.* 19:13–25.
61. Isralewitz, B., M. Gao, and K. Schulten. 2001. Steered molecular dynamics and mechanical functions of proteins. *Curr. Opin. Struct. Biol.* 11:224–230.
62. Gao, M., M. Sotomayor, E. Villa, E. Lee, and K. Schulten. 2006. Molecular mechanisms of cellular mechanics. *Phys. Chem. Chem. Phys.* 8:3692–3706.
63. Sotomayor, M., and K. Schulten. 2007. Single-molecule experiments in vitro and in silico. *Science.* 316:1144–1148.
64. Gräter, F., J. Shen, H. Jiang, M. Gautel, and H. Grubmüller. 2005. Mechanically induced titin kinase activation studied by force-probe molecular dynamics simulations. *Biophys. J.* 88:790–804.
65. Lee, E. H., J. Hsin, O. Mayans, and K. Schulten. 2007. Secondary and tertiary structure elasticity of titin Z1Z2 and a titin chain model. *Biophys. J.* 93:1719–1735.
66. Lee, G., K. Abdi, Y. Jiang, P. Michaely, V. Bennett, and P. E. Marszalek. 2006. Nanospring behavior of ankyrin repeats. *Nature.* 440:246–249.
67. Michaely, P., D. R. Tomchick, M. Machius, and R. G. W. Anderson. 2002. Crystal structure of a 12 ANK repeat stack from human ankyrin-R. *EMBO J.* 21:6387–6396.
68. Silver, F. H., D. Christiansen, P. B. Snowhill, Y. Chen, and W. J. Landis. 2000. The role of mineral in the storage of elastic energy in turkey tendons. *Biomacromolecules.* 1:180–185.
69. Izrailev, S., S. Stepaniants, M. Balsera, Y. Oono, and K. Schulten. 1997. Molecular dynamics study of unbinding of the avidin-biotin complex. *Biophys. J.* 72:1568–1581.
70. Evans, E., and K. Ritchie. 1997. Dynamic strength of molecular adhesion bonds. *Biophys. J.* 72:1541–1555.
71. Lu, H., B. Isralewitz, A. Krammer, V. Vogel, and K. Schulten. 1998. Unfolding of titin immunoglobulin domains by steered molecular dynamics simulation. *Biophys. J.* 75:662–671.
72. Marszalek, P. E., H. Lu, H. Li, M. Carrion-Vazquez, A. F. Oberhauser, K. Schulten, and J. M. Fernandez. 1999. Mechanical unfolding intermediates in titin modules. *Nature.* 402:100–103.
73. Krammer, A., H. Lu, B. Isralewitz, K. Schulten, and V. Vogel. 1999. Forced unfolding of the fibronectin type III module reveals a tensile molecular recognition switch. *Proc. Natl. Acad. Sci. USA.* 96:1351–1356.
74. Lu, H., and K. Schulten. 1999. Steered molecular dynamics simulation of conformational changes of immunoglobulin domain I27 interpret atomic force microscopy observations. *Chem. Phys.* 247:141–153.
75. Gao, M., D. Craig, V. Vogel, and K. Schulten. 2002. Identifying unfolding intermediates of FN-III₁₀ by steered molecular dynamics. *J. Mol. Biol.* 323:939–950.
76. Gao, M., D. Craig, O. Lequin, I. D. Campbell, V. Vogel, and K. Schulten. 2003. Structure and functional significance of mechanically unfolded fibronectin type III intermediates. *Proc. Natl. Acad. Sci. USA.* 100:14784–14789.
77. Craig, D., M. Gao, K. Schulten, and V. Vogel. 2004. Tuning the mechanical stability of fibronectin type III modules through sequence variation. *Structure.* 12:21–30.
78. Lu, H., and K. Schulten. 1999. Steered molecular dynamics simulations of force-induced protein domain unfolding. *Proteins Struct. Funct. Genet.* 35:453–463.
79. Howard, J. 2001. *Mechanics of Motor Proteins and the Cytoskeleton*. Sinauer Associates, Sunderland, MA.
80. Hynes, R. O. 2002. Integrins: bidirectional, allosteric signaling machines. *Cell.* 110:673–687.
81. Patel, S. D., C. Ciatto, C. P. Chen, F. Bahna, N. A. Rajebhosale, I. Schieren, T. M. Jessell, B. Honig, S. R. Price, and L. Shapiro. 2006. Type II cadherin ectodomain structures: implications for classical cadherin specificity. *Cell.* 124:1255–1268.
82. Concha, N. O., J. F. Head, M. A. Kaetzel, J. R. Dedman, and B. A. Seaton. 1993. Rat annexin V crystal structure: Ca²⁺-induced conformational changes. *Science.* 261:1321–1324.
83. Sopkova, J., M. Renouard, and A. Lewit-Bentley. 1993. The crystal structure of a new high-calcium form of annexin V. *J. Mol. Biol.* 234:816–825.
84. He, W., P. Cowin, and D. L. Stokes. 2003. Untangling desmosomal knots with electron tomography. *Science.* 302:109–113.
85. Chen, C. P., S. Posy, A. Ben-Shaul, L. Shapiro, and B. H. Honig. 2005. Specificity of cell-cell adhesion by classical cadherins: critical role for low-affinity dimerization through β -strand swapping. *Proc. Natl. Acad. Sci. USA.* 102:8531–8536.

86. Prakasam, A. K., V. Maruthamuthu, and D. E. Leckband. 2006. Similarities between heterophilic and homophilic cadherin adhesion. *Proc. Natl. Acad. Sci. USA.* 103:15434–15439.
87. Bork, J. M., L. M. Peters, S. Riazuddin, S. L. Bernstein, Z. M. Ahmed, S. L. Ness, R. Polomeno, A. Ramesh, M. Schloss, C. R. S. Srisailpathy, S. Wayne, S. Bellman, D. Desmukh, Z. Ahmed, S. N. Khan, V. M. der Kaloustian, X. C. Li, A. Lalwani, S. Riazuddin, M. Bitner-Glindzicz, W. E. Nance, X.-Z. Liu, G. Wistow, R. J. H. Smith, A. J. Griffith, E. R. Wilcox, T. B. Friedman, and R. J. Morell. 2001. Usher syndrome 1D and nonsyndromic autosomal recessive deafness DFNB12 are caused by allelic mutations of the novel cadherin-like gene CDH23. *Am. J. Hum. Genet.* 68:26–37.
88. de Brouwer, A. P. M., R. J. Pennings, M. Roeters, P. van Hauwe, L. M. Astuto, L. H. Hoefsloot, P. L. M. Huygen, B. van den Helm, A. F. Deutman, J. M. Bork, W. J. Kimberling, F. P. M. Cremers, C. W. R. J. Cremers, and H. Kremer. 2003. Mutations in the calcium-binding motifs of CDH23 and the 35DELG mutation in *gjb2* cause hearing loss in one family. *Hum. Genet.* 112:156–163.
89. Mirijanian, D. T., J. W. Chu, G. S. Ayton, and G. A. Voth. 2007. Atomistic and coarse-grained analysis of double spectrin repeat units: the molecular origins of flexibility. *J. Mol. Biol.* 365:523–534.
90. Paramore, S., and G. A. Voth. 2006. Examining the influence of linkers and tertiary structure in the forced unfolding of multiple-repeat spectrin molecules. *Biophys. J.* 91:3436–3445.
91. Marino, M., P. Zou, D. Svergun, P. Garcia, C. Edlich, B. Simon, M. Wilmanns, C. Muhle-Goll, and O. Mayans. 2006. The Ig doublet Z1Z2: a model system for the hybrid analysis of conformational dynamics in Ig tandems from titin. *Structure.* 14:1437–1447.